Higher-Order Sinusoidal-Input Describing Function Analysis of Fractional-Order Hybrid Integrator-Gain Systems [★]

S. Ali Hosseini [*] **Luke F. van Eijk** [*,**] **Marcin B. Kaczmarek** [*]
S. Hassan HosseinNia [*]

[*] *Department of Precision and Microsystems Engineering, Delft University of Technology, 2628 CD Delft, The Netherlands (e-mail: (s.a.hosseini, l.f.vaneijk, m.b.kaczmarek, s.h.hosseinniakani)@tudelft.nl).*
[**] *ASMPT, 6641 TL Beuningen, The Netherlands.*

Abstract: In this paper, the higher-order sinusoidal-input describing function (HOSIDF) of the fractional-order hybrid integrator-gain system (HIGS) is derived analytically. The HIGS element, designed as a nonlinear component, aims to overcome limitations inherent in linear control, such as the waterbed effect. The HIGS element has been generalized by replacing the integer-order integrator with a fractional one. Here, a modified version of the fractional-order HIGS (FO-HIGS) is introduced with the aim of shaping the nonlinearity at low frequencies. Additionally, this paper demonstrates that obtaining an analytical solution for the HOSIDF of the FO-HIGS enables us to gain better insight into the tuning of the control architecture.

Keywords: Hybrid integrator-gain systems, Frequency domain analysis, Fractional-order systems, Higher-order sinusoidal-input describing function, PID controllers.

1. INTRODUCTION

The main drawback of linear time-invariant (LTI) controllers are their fundamental limitations like the waterbed effect and Bode's gain-phase relationship, as seen in Freudenberg et al. (2000). The fundamental limitations can be relaxed by applying a nonlinear element to control an LTI plant. This approach has been followed using both hybrid systems and more general nonlinearities. Overcoming the fundamental limitations has been shown using reset controllers, hybrid integrator-gain system (HIGS)-based controllers, and variable-gain controllers, see, e.g., Zhao et al. (2019); van Dinther et al. (2021); Hunnekens et al. (2016). Utilizing nonlinear elements that can be described in the frequency domain to create a viable alternative to LTI controllers is highly beneficial. This is especially crucial given the complexity of industrial devices, where the plant's measured frequency-response function (FRF) often represents the most precise existing information.

A comparative overview of frequency domain methods for nonlinear systems is presented in Rijlaarsdam et al. (2017). Methods like sinusoidal-input describing function (SIDF) and higher-order SIDF (HOSIDF), are presented to approximate nonlinear elements in the frequency domain, see Nuij et al. (2006). In the SIDF approach, the steady-state response of a convergent nonlinear system (Pavlov et al., 2004), is represented by the first component of the Fourier series expansion, while the higher components are considered in the HOSIDF analysis to provide additional insights into the behavior of a nonlinear system.

An example of a nonlinear controller analyzed in the frequency domain is the Constant in gain, Lead in phase (CgLp) element. In Saikumar et al. (2019), a reset-based CgLp element is suggested as a remedy for Bode's gain-phase relationship. Similar to the reset element, HIGS also holds the potential for overcoming the limitations of LTI controllers (Deenen et al., 2017). Furthermore, the sector-boundedness of the HIGS element provides us with the opportunity to explore the development of a circle criterion-like frequency-domain stability method for a HIGS-based control system (Deenen et al., 2021).

Like the reset element, HIGS also generates higher-order harmonics in its output for all input frequencies, presented in van Eijk et al. (2023). In van Eijk et al. (2023), the HIGS element is generalized by placing it in parallel with a linear low-pass filter to shape the higher-order harmonics. In Hosseini et al. (2022), the HIGS element is also generalized with the aim to further suppress HOSIDFs by replacing the integer-order integrator of HIGS with a fractional-order one. With both generalizations, it becomes possible to tune the phase of the SIDF as well as the influence of higher-order harmonics. In this work, we modify the nonlinear element developed in Hosseini et al. (2022) such that it does not produce any higher-order harmonics below a certain threshold frequency.

To this respect, the main contributions of this paper are:

- Modifying the definition of the FO-HIGS by introducing an additional condition within the upper gain-region, which is one of the two gain-regions of the FO-HIGS element. This adjustment aims to maintain the output within the upper gain-region below a certain threshold frequency, which leads to an element with no higher-order harmonics at those frequencies.

466

- Introducing the analytic formula for the HOSIDFs of FO-HIGS, enabling a more comprehensive analysis of its frequency-domain properties.
- Designing two CgLp elements using conventional HIGS and FO-HIGS, and investigating the presence of higher-order harmonics in a closed-loop control system involving these elements.

The structure of the paper is as follows. In Section 2, preliminary information is presented. In Section 3, the modified version of the FO-HIGS is introduced, and the analytical solution for its HOSIDF is derived. In Section 4, HIGS-based CgLp and FO-HIGS-based CgLp elements are presented, as well as their frequency domain responses. In Section 5, the performance of FO-HIGS is compared with HIGS and PID when controlling a second-order system. Section 6 states the conclusions and future works.

2. PRELIMINARIES

2.1 Describing function

The SIDF ($\mathscr{D}_1(\omega, \hat{e})$) is a quasi-linearization of a nonlinear element subject to a sinusoidal input $\bar{e}(t) = \hat{e}\sin(\omega t)$, with amplitude $\hat{e} \in \mathbb{R}_{>0}$, excitation frequency $\omega \in \mathbb{R}_{>0}$, and time $t \in \mathbb{R}$. The SIDF has also been extended to the nth-order SIDF or HOSIDF ($\mathscr{D}_n(\omega, \hat{e})$) in Nuij et al. (2006). Considering the output of a nonlinear system converging to a (unique) solution $\bar{u}$ which is periodic with the same period $T = \frac{2\pi}{\omega}$ as the sinusoidal input, then it can be presented as the SIDF and HOSIDF of the nonlinear element as follows

$$\bar{u}(t) = \sum_{n=1}^{\infty} |\mathscr{D}_n(\omega, \hat{e})| \sin\left(n\omega t + \angle\mathscr{D}_n(\omega, \hat{e})\right), \quad (1)$$

where as shown in Nuij et al. (2006), this n^{th}-order SIDF is given by

$$\mathscr{D}_n(\omega, \hat{e}) = b_n + ja_n, \quad (2)$$

with Fourier coefficients

$$a_n = \frac{2}{T} \int_0^T \frac{1}{\hat{e}} \bar{u}(t)\cos(n\omega t)\mathrm{d}t, \quad (3a)$$

$$b_n = \frac{2}{T} \int_0^T \frac{1}{\hat{e}} \bar{u}(t)\sin(n\omega t)\mathrm{d}t, \quad (3b)$$

and $j = \sqrt{-1}$.

2.2 Fractional-order derivative

The Liouville-Caputo (LC) fractional-order derivative, which is used for FO-HIGS, is defined as (Shchedrin et al., 2018)

$$^{\text{LC}}D_x^\eta f(x) := \frac{1}{\Gamma(1-\eta)} \int_{-\infty}^x \mathrm{d}t(x-t)^{-\eta}\frac{\mathrm{d}f(t)}{\mathrm{d}t}, \quad (4)$$

where $\eta \in [0,1]$ is the derivative order, $x \in \mathbb{R}$ is the upper-bound of the integral, and $\Gamma(.)$ is the Euler Gamma function, defined as

$$\Gamma(z) = \int_0^\infty e^{-t}t^{z-1}\mathrm{d}t, \quad (5)$$

where $z \in \mathbb{C}$, and Real$(z) > 0$. According to Shchedrin et al. (2018), for a sinusoidal function $f(t)$ we have

$$^{\text{LC}}D_t^\eta[\sin(\omega t)] = \omega^\eta \sin\left(\omega t + \frac{\pi\eta}{2}\right). \quad (6)$$

For convenience in the following, writing LC in $^{\text{LC}}D_x^\eta$ will be refrained.

3. FO-HIGS, FROM MODIFIED DEFINITION TO HOSIDF FORMULA

In this section, the FO-HIGS in Hosseini et al. (2022) is modified. In Section 3.1, we propose an additional condition aiming to maintain the FO-HIGS within the upper gain-region below a certain frequency, thereby preventing premature departure and eliminating higher-order harmonics. In Section 3.2, the HOSIDF of the FO-HIGS is derived analytically.

3.1 FO-HIGS definition

We define the FO-HIGS in state-space representation as

$$\mathcal{H}_f^\alpha : \begin{cases} \dot{x}_h(t) = \omega_h D_t^{1-\alpha}e(t), & \text{if } (e(t), \dot{e}(t), u(t)) \in \mathcal{F}_1^\alpha, \\ x_h(t) = k_h e(t), & \text{if } (e(t), \dot{e}(t), u(t)) \in \mathcal{F}_2^\alpha, \\ x_h(t) = 0, & \text{if } (e(t), \dot{e}(t), u(t)) \in \mathcal{F}_3^\alpha, \\ u(t) = x_h(t), \end{cases}$$
$$(7)$$

where $x_h \in \mathbb{R}$ is the state variable, $u \in \mathbb{R}$ is the output, $e \in \mathbb{R}$ is the input, $k_h \in \mathbb{R}_{>0}$ is the gain value, $\omega_h \in \mathbb{R}_{>0}$ is the integrator frequency, and $\alpha \in [0,1]$ is the integration order. The FO-HIGS can operate in three different regions, where the integrator-region is

$$\mathcal{F}_1^\alpha = \mathcal{F} \setminus (\mathcal{F}_2^\alpha \cup \mathcal{F}_3^\alpha), \quad (8)$$

the upper gain-region is

$$\mathcal{F}_2^\alpha := \Big\{(e, \dot{e}, u) \in \mathcal{F} \,|\, u = k_h e \,\wedge\, \big(\omega_h D_t^{1-\alpha}(e)e > k_h\dot{e}e...$$
$$\vee\, D_t^{1-\alpha}(e)e < 0 \,\vee\, (e = 0 \,\wedge\, \omega_h D_t^{1-\alpha}(e)\dot{e} > k_h\dot{e}^2))\Big\},$$
$$(9)$$

the lower gain-region is

$$\mathcal{F}_3^\alpha = \Big\{(e, \dot{e}, u) \in \mathcal{F} \,|\, u = 0 \,\wedge\, \Big[D_t^{1-\alpha}(e)e < 0 \,\vee\, ...$$
$$\Big(e = 0 \,\wedge\, \big(D_t^{1-\alpha}(e)\dot{e} < 0 \,\vee\, (\dot{e} = 0 \,\wedge\, D_t^{1-\alpha}(e) \neq 0))\big)\Big)\Big]\Big\},$$
$$(10)$$

and

$$\mathcal{F} := \left\{(e, \dot{e}, u) \in \mathbb{R}^3 \,|\, eu \geq \frac{1}{k_h}u^2\right\}. \quad (11)$$

The three regions are created in such a way that FO-HIGS is bounded within region $\mathcal{F}$ and has a continuous output signal. A derivation of these conditions, except the newly added condition $u = k_h e \wedge D_t^{1-\alpha}(e)e < 0$ to the upper gain-region $\mathcal{F}_2^\alpha$, can be found in Hosseini et al. (2022). The new condition has been added to upper gain-region $\mathcal{F}_2^\alpha$ to prevent premature departure from the upper gain-region for a sinusoidal input, as explained in Section 3.2. The output of FO-HIGS for a sinusoidal input $e(t) = \sin(t)$ is depicted in Fig. 1. It can be seen that by decreasing α from 1 to 0, the output gradually goes from the behaviour of a HIGS to that of a proportional gain. Also, it can be seen that the output of FO-HIGS is bounded between 0 and $k_h e(t)$.

3.2 HOSIDF of FO-HIGS

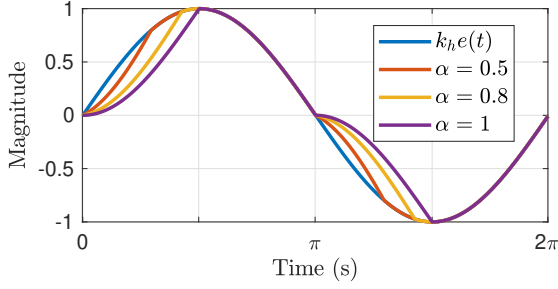To derive the FO-HIGS's HOSIDF formula, it is necessary to compute its steady-state response to a sinusoidal input.

Fig. 1. Output response of FO-HIGS when subject to a sinusoidal input $e(t) = \sin(t)$, with $\omega_h = 1$, $k_h = 1$, and various values for α.

Let's consider $e(t) = \hat{e}\sin(\omega t)$ as the input and $u(t)$ as the output of the system (7), where $t \in [0, \frac{2\pi}{\omega}]$. It is defined here that the frequency ω_{L} marks the point where $\dot{x}_h(0)$ from the integrator-mode equals $\dot{x}_h(0)$ from the upper gain-mode. Considering the conditions in (8)-(10), if $\omega > \omega_{\mathrm{L}}$, the FO-HIGS initiates in the integrator-mode, while for $\omega \leq \omega_{\mathrm{L}}$, it begins in the upper gain-mode.

For the case where FO-HIGS initiates from the integrator mode ($\omega > \omega_{\mathrm{L}}$), $\omega t = \gamma$ marks the point at which the system switches to the upper gain-mode. Considering the conditions in (9), the system remains in this mode until $k_h\hat{e}\sin(\omega t)$ intersects the zero line at $\omega t = \pi$. This pattern is also demonstrable for the subsequent half cycle ($\omega t \in [\pi, 2\pi]$). The switching point γ, is calculated in Hosseini et al. (2022) as below

$$\gamma = -2\arctan\left(\frac{\cos(\frac{\pi\alpha}{2}) - \frac{k_h\omega^\alpha}{\omega_h}}{\sin(\frac{\pi\alpha}{2})}\right), \quad (12)$$

where by setting $\gamma = 0$ and solving it for ω, the frequency ω_{L} is derived as

$$\omega_{\mathrm{L}} = \left(\frac{\omega_h}{k_h}\cos\left(\frac{\pi\alpha}{2}\right)\right)^{1/\alpha}. \quad (13)$$

Thus, for $\omega > \omega_{\mathrm{L}}$, the FO-HIGS is in the integrator-region for $t \in [0, \frac{\gamma}{\omega})$, and then moves to the upper gain-region. First, we will demonstrate that it remains there within the range of $t \in [\frac{\gamma}{\omega}, \frac{\pi}{2\omega})$ by showing that $\dot{x}_h(t)$ from the integrator-mode stays greater than $\dot{x}_h(t)$ from the upper gain-mode. Therefore, we expect the inequality

$$D_t^{1-\alpha}\omega_h e(t) > k_h\dot{e}(t), \quad (14)$$

to hold for $t \in [\frac{\gamma}{\omega}, \frac{\pi}{2\omega})$. By substituting $e(t) = \sin(\omega t)$, the inequality in (14) can be simplified as below

$$\omega t > \arctan\left(\frac{\frac{k_h\omega^\alpha}{\omega_h} - \cos\left(\frac{\pi\alpha}{2}\right)}{\sin\left(\frac{\pi\alpha}{2}\right)}\right), \quad (15)$$

by considering γ from (12), we have

$$t > \frac{1}{2}\frac{\gamma}{\omega}, \quad (16)$$

which means the inequality (14) holds for $t \in [\frac{\gamma}{\omega}, \frac{\pi}{2\omega})$. However, staying in the upper gain-region cannot be guaranteed for $t \in [\frac{\pi}{2\omega}, \frac{\pi}{\omega})$. Leaving the upper gain-region means $D_t^{1-\alpha}\omega_h e(t) < k_h\dot{e}(t)$, where for the interval $t \in [\frac{\pi}{2\omega}, \frac{\pi}{\omega})$, $\dot{e}(t) \leq 0$. Therefore, by preventing the negative values for $\dot{x}_h(t)$ in the integrator-mode, we can always guarantee $D_t^{1-\alpha}\omega_h e(t) > k_h\dot{e}(t)$. In this respect, the new condition ($u = k_he \wedge D_t^{1-\alpha}(e)e < 0$) has been added to the upper gain-region $\mathcal{F}_2^\alpha$. The same is true for the next half

period $[\frac{\pi}{\omega}, \frac{2\pi}{\omega}]$.

Hence, the FO-HIGS's steady-state response for $\omega > \omega_{\mathrm{L}}$ is given by

$$u(t) = \begin{cases} \frac{\omega_h}{\omega^\alpha}\hat{e}\left(\sin(\omega t - \frac{\pi\alpha}{2}) + \sin(\frac{\pi\alpha}{2})\right), & 0 \leq t < \frac{\gamma}{\omega}, \\ k_h\hat{e}\sin(\omega t), & \frac{\gamma}{\omega} \leq t < \frac{\pi}{\omega}, \\ \frac{\omega_h}{\omega^\alpha}\hat{e}\left(\sin(\omega t - \frac{\pi\alpha}{2}) - \sin(\frac{\pi\alpha}{2})\right), & \frac{\pi}{\omega} \leq t < \frac{\gamma+\pi}{\omega}, \\ k_h\hat{e}\sin(\omega t), & \frac{\gamma+\pi}{\omega} \leq t < \frac{2\pi}{\omega}. \end{cases} \quad (17)$$

For $\omega \leq \omega_{\mathrm{L}}$, the FO-HIGS initially operates in the upper gain region. In the interval $t \in [0, \frac{\pi}{2\omega})$, inequality (14) must be satisfied, which consequently leads to inequality (15). Given $\omega \leq \omega_{\mathrm{L}}$, replacing ω_{L} from (13) with ω on the right side of the inequality in (15) results in $\omega t > 0$. Therefore, within the interval $t \in [0, \frac{\pi}{2\omega})$, the FO-HIGS cannot exit the upper gain-region. For the range $t \in [\frac{\pi}{2\omega}, \frac{\pi}{\omega})$, similar to the scenario when $\omega > \omega_{\mathrm{L}}$, it is essential to avoid negative values for $\dot{x}_h(t) = D_t^{1-\alpha}(e)$ of the integrator-mode. In this respect, the condition ($u = k_he \wedge D_t^{1-\alpha}(e)e < 0$) will prevent departing from the upper gain-region. In conclusion, when the FO-HIGS starts from its upper gain-region, it will remain there till $t = \frac{\pi}{\omega}$. For the next half cycle, the same happens. Hence, in case $\omega \leq \omega_{\mathrm{L}}$, the output of the FO-HIGS is always equal to $k_h\hat{e}\sin(\omega t)$.

The below theorem expresses the HOSIDF of FO-HIGS.

Theorem 1. The HOSIDF formula for FO-HIGS is as follows

$$\mathscr{H}_n^\alpha(\omega) = b_n + ja_n, \quad (18)$$

where α is the order of the fractional integrator, and $n \in \mathbb{N}$ is the order of the harmonic. For $\omega \leq \omega_{\mathrm{L}}$

$$a_1 = 0, \quad b_1 = k_h, \quad (19)$$

and

$$a_n = 0, \quad b_n = 0, \quad \forall n \geq 2. \quad (20)$$

For $\omega > \omega_{\mathrm{L}}$, a_n and b_n are as in (21)-(23).

Proof. For the case where $\omega \leq \omega_{\mathrm{L}}$ we have $u(t) = k_h\hat{e}\sin(\omega t)$, then for a_1 and b_1 we have

$$a_1 = \frac{2}{T}\int_0^T k_h\sin(\omega t)\cos(\omega t)\mathrm{d}t = 0, \quad (24a)$$

$$b_1 = \frac{2}{T}\int_0^T k_h\sin(\omega t)\sin(\omega t)\mathrm{d}t = k_h, \quad (24b)$$

and for a_n and b_n ($n \geq 2$)

$$a_n = \frac{2}{T}\int_0^T k_h\sin(\omega t)\cos(n\omega t)\mathrm{d}t = 0, \quad (25a)$$

$$b_n = \frac{2}{T}\int_0^T k_h\sin(\omega t)\sin(n\omega t)\mathrm{d}t = 0. \quad (25b)$$

When $\omega > \omega_{\mathrm{L}}$, substitute the steady-state response from (17) as $\bar{u}(t)$ into (3). Next is calculating the integral over the interval $[0, T]$, where $T = \frac{2\pi}{\omega}$. This computation yields the values for a_n and b_n as expressed in (21) [1]-(23). ∎

Definition 1. Considering $\mathscr{H}_1^\alpha(\omega)$ as the SIDF of the FO-HIGS for $\omega > \omega_{\mathrm{L}}$, the cut-off frequency (ω_r) of this filter is defined as the frequency at which the equation

---

[1] It is worth noting that the SIDF for FO-HIGS in Hosseini et al. (2022) requires multiplication by two due to a typographical error in the definition of a_1 and b_1. The authors acknowledge this oversight and provide the corrected version in (21).

$$a_1 = \frac{\omega_h}{2\pi\omega^\alpha}\left[-\cos\left(2\gamma - \frac{\pi\alpha}{2}\right) + \cos\left(\frac{\pi\alpha}{2}\right) - 2\gamma\sin\left(\frac{\pi\alpha}{2}\right) + 2\cos\left(\gamma - \frac{\pi\alpha}{2}\right) - 2\cos\left(\gamma + \frac{\pi\alpha}{2}\right)\right] + \frac{k_h}{2\pi}[\cos(2\gamma) - 1], \quad (21a)$$

$$b_1 = \frac{\omega_h}{2\pi\omega^\alpha}\left[2\gamma\cos\left(\frac{\pi\alpha}{2}\right) - \sin\left(2\gamma - \frac{\pi\alpha}{2}\right) + 3\sin\left(\frac{\pi\alpha}{2}\right) - 2\sin\left(\gamma + \frac{\pi\alpha}{2}\right) + 2\sin\left(\gamma - \frac{\pi\alpha}{2}\right)\right] + \frac{k_h}{2\pi}[2\pi - 2\gamma + \sin(2\gamma)], \quad (21b)$$

$$a_n = -\frac{\omega_h}{\pi(n+1)\omega^\alpha}\left[\cos\left((n+1)\gamma - \frac{\pi\alpha}{2}\right) - \cos\left(\frac{\pi\alpha}{2}\right)\right] - \frac{\omega_h}{\pi(1-n)\omega^\alpha}\left[\cos\left((1-n)\gamma - \frac{\pi\alpha}{2}\right) - \cos\left(\frac{\pi\alpha}{2}\right)\right]$$
$$+ \frac{\omega_h}{\pi n\omega^\alpha}\left[\cos\left(n\gamma - \frac{\pi\alpha}{2}\right) - \cos\left(n\gamma + \frac{\pi\alpha}{2}\right)\right] - \frac{k_h}{\pi(n+1)}\left[1 - \cos\left((n+1)\gamma\right)\right] - \frac{k_h}{\pi(1-n)}\left[1 - \cos\left((1-n)\gamma\right)\right], \qquad \forall\,\text{odd}\,n \geq 2, \quad (22a)$$

$$b_n = -\frac{\omega_h}{\pi(n+1)\omega^\alpha}\left[\sin\left((n+1)\gamma - \frac{\pi\alpha}{2}\right) + \sin\left(\frac{\pi\alpha}{2}\right)\right] + \frac{\omega_h}{\pi(1-n)\omega^\alpha}\left[\sin\left((1-n)\gamma - \frac{\pi\alpha}{2}\right) + \sin\left(\frac{\pi\alpha}{2}\right)\right]$$
$$+ \frac{\omega_h}{\pi n\omega^\alpha}\left[\sin\left(n\gamma - \frac{\pi\alpha}{2}\right) - \sin\left(n\gamma + \frac{\pi\alpha}{2}\right) + 2\sin\left(\frac{\pi\alpha}{2}\right)\right] + \frac{k_h}{\pi(n+1)}\left[\sin\left((n+1)\gamma\right)\right] - \frac{k_h}{\pi(1-n)}\left[\sin\left((1-n)\gamma\right)\right], \quad \forall\,\text{odd}\,n \geq 2, \quad (22b)$$

$$a_n = 0, \quad b_n = 0, \quad \forall\,\text{even}\,n \geq 2. \quad (23)$$
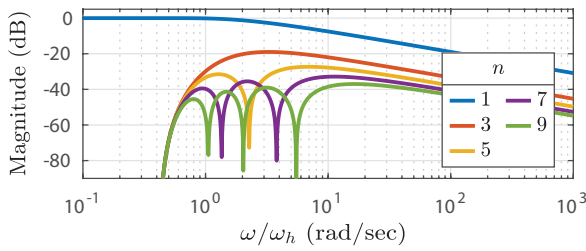

Fig. 2. HOSIDF of FO-HIGS with $k_h = 1$, $\omega_h = 1$, and $\alpha = 0.6$. From (27), the cut-off frequency $\omega_r = 2.69\,\text{rad/s}$.

$$\lim_{\omega\to\infty}|\mathscr{H}_1^\alpha(\omega)| = \lim_{\omega\to 0}|\mathscr{H}_1^\alpha(\omega)|, \quad (26)$$

is satisfied. Then, for ω_r, this relationship yields

$$\omega_r = \left(\frac{\omega_h}{k_h}\left|(4/\pi - j)\sin\left(\frac{\alpha\pi}{2}\right) + \cos\left(\frac{\alpha\pi}{2}\right)\right|\right)^{\frac{1}{\alpha}}. \quad (27)$$

The magnitudes of the first and higher-order harmonics of FO-HIGS with $\alpha = 0.6$ are depicted in Fig. 2. It can be seen that the higher-order harmonics are not produced below a specific frequency, and for the same parameters, they all share the same $\omega_\text{L} = 0.41\,\text{rad/s}$. Moreover, the notches in the HIGS's HOSIDFs (van Eijk et al., 2023) can also be observed in the FO-HIGS HOSIDFs.

4. FO-HIGS-BASED CGLP ELEMENTS

An element with adjustable phase lag and magnitude characteristics of a linear low-pass filter can be created using HIGS in either a parallel or series interconnection with LTI elements. A CgLp element can be formed by arranging these structures in series with a lead component. In Fig. 3, a HIGS and FO-HIGS-based CgLp element is presented. Placing a lead in front of a nonlinear element (Cai et al., 2020; van den Eijnden et al., 2020) has proven beneficial for transient response, while it does not affect the first harmonic. We used the same rationale to place the lead first in our design.

4.1 Parallel architecture

The parallel generalized HIGS is introduced in Hosseini et al. (2022) and van Eijk et al. (2023). Responses of a linear low-pass filter

$$F(s) = \frac{1}{s/\omega_r + 1}, \quad (28)$$

with corner-frequency $\omega_r \in \mathbb{R}_{>0}$ and corresponding integer-order HIGS are combined with ratio $\beta \in [0, 1]$. The parameters for HIGS are considered as $\alpha = 1$, $k_h = 1$ and ω_h will be derived from (27) by substituting the arbitrary value for ω_r. $\beta = 0$ and $\beta = 1$ lead to pure linear and nonlinear responses, respectively. In this case, a linear integer-order lead element

$$L(s) = \frac{s/\omega_r + 1}{s/\omega_f + 1}, \quad (29)$$

is combined with the parallel structure. The low-pass filter $\frac{1}{s/\omega_f + 1}$, with $\omega_f \in \mathbb{R}_{>0}$ and $\omega_f \gg \omega_r$, is added to ensure that $L(s)$ is a proper transfer function. The HOSIDF of this structure is given by (Karbasizadeh, 2023, Chapter 10)

$$G_n^\text{p}(j\omega) = \begin{cases} L(j\omega)\left(\beta\mathscr{H}_n^1(\omega) + (1-\beta)F(j\omega)\right), & \text{for } n = 1, \\ L(j\omega)e^{j(n-1)\angle L(j\omega)}\beta\mathscr{H}_n^\alpha(\omega), & \text{for } n \geq 2. \end{cases} \quad (30)$$

4.2 Series architecture

In the series architecture, a fractional-order lead filter

$$L^\alpha(s) = \frac{(s/\omega_r + 1)^\alpha}{(s/\omega_f + 1)^\alpha}, \quad (31)$$

is followed by FO-HIGS to create the CgLp element in Fig. 3b. Its HOSIDF can be calculated as follows

$$G_n^\text{s}(j\omega) = L^\alpha(j\omega)e^{j(n-1)\angle L^\alpha(j\omega)}\mathscr{H}_n^\alpha(\omega). \quad (32)$$

Fig. 4 illustrates the SIDF and third-order SIDF of a HIGS and FO-HIGS-based CgLp element. It is noticeable that the third-order SIDFs of the two architectures are different, especially at low frequencies. Moreover, based on FO-HIGS's SIDF, varying values of α result in distinct phases of SIDF. Therefore, when α is fixed, the parameter β is adjusted to demonstrate a phase behavior similar to that of an FO-HIGS-based CgLp element for a desired frequency range.

5. ILLUSTRATIVE EXAMPLE

In this section, an example is employed to demonstrate how the attained phase lead from CgLp elements, arising

(a) Parallel architecture (Case 1)
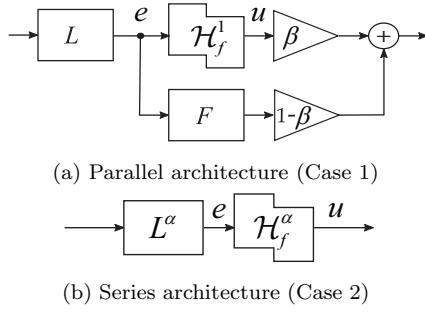

(b) Series architecture (Case 2)

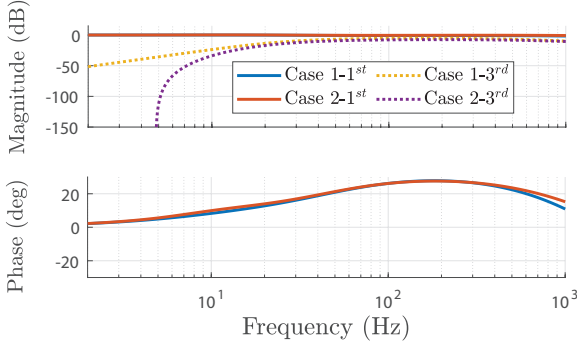Fig. 3. Architectures for HIGS-based CgLp element.

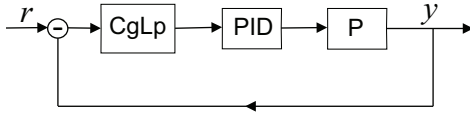Fig. 4. First and third-order SIDF for the two CgLp cases.

Fig. 5. Block diagram of the closed-loop system.

from the two structures, can enhance tracking performance when incorporated into a PID controller. Also, the differences between the two proposed structures regarding their higher-order harmonics are investigated.

The closed-loop structure consists of the CgLp element in series with the PID controller and the plant, as shown in Fig. 5. A second-order mass-spring-damper system, modeled in Saikumar et al. (2019) based on a precision planar positioning stage, is considered as the plant in this study and is given by the following transfer function

$$\mathrm{P}(s) = \frac{104.996}{\frac{s^2}{\omega_n^2} + \frac{2\zeta s}{\omega_n} + 1}, \qquad (33)$$

where $\omega_n = 87.962$ and $\zeta = 0.25$.

5.1 Controller design using CgLp elements

Three different controllers are designed to provide 30° phase lead at the bandwidth frequency $\omega_c = 2\pi \times 100\,\mathrm{rad/sec}$. Initially, the entire phase lead is supplied by the PID controller

$$C_{\mathrm{PID}}(s) = K_p \left(1 + \frac{\omega_i}{s}\right) \left(\frac{1 + \frac{s}{\omega_d}}{1 + \frac{s}{\omega_t}}\right), \qquad (34)$$

where a low-pass filter is added to the pure PID controller case because other CgLp elements also have a low-pass filter. Therefore, we have

$$C_1(s) = C_{\mathrm{PID}}(s) \times \left(\frac{1}{1 + \frac{s}{\omega_f}}\right), \qquad (35)$$

with $\omega_f = 2\pi \times 2000\,\mathrm{rad/sec}$. The tuning procedure follows the rule of thumb method described in Munnig Schmidt et al. (2020). Here, $K_p \in \mathbb{R}$ represents the PID gain, ensuring zero dB gain at bandwidth frequency ω_c, $\omega_i = \omega_c/10$ is the frequency at which integral action is stopped, differentiating action is started at $\omega_d = \omega_c/a$ and terminated at $\omega_t = a\omega_c$, where we choose $a = 2.12$ to have 30° phase lead at the bandwidth frequency.

Two additional controllers are configured as CgLp-PID controllers, comprising the CgLp elements in Fig. 3, in series with a PID. Based on the phase advantage of the CgLp elements, we attempted to provide most of the required phase from the CgLp elements. Therefore, the parameters for PID are adjusted to provide only 4° phase lead, and the CgLp part is tuned to provide 26° phase lead at the bandwidth frequency. The structure of the PID element in the CgLp-PID controllers remains identical to (34) and is tuned according to the same rules of thumb but with $a = 1.2$. Therefore, the other controllers are as

$$C_2 = \mathrm{Case1} \times C_{\mathrm{PID}}, \qquad (36)$$

and

$$C_3 = \mathrm{Case2} \times C_{\mathrm{PID}}, \qquad (37)$$

where the parameters for Case 1 (parallel architecture) and Case 2 (series architecture) are arbitrarily set as $\alpha = 0.7$, $\beta = 0.73$, and $\omega_r = 2\pi \times 35\,\mathrm{rad/sec}$, to provide the same phase at the bandwidth frequency. The corresponding ω_h for each case can be calculated using (27).

5.2 Results

In the previous subsection, three controllers were designed to share the same phase margin and bandwidth frequency. By using the nonlinear CgLp element in Cases 1 and 2, we could achieve more gain at low frequencies, which is desired in most control applications. Note that the same procedure can be done by applying these CgLp elements to every PID controller with different parameters. In Fig. 6, the step responses for all three controllers are depicted. Upon examining the overshoot, both HIGS and FO-HIGS have demonstrated superior performance compared to linear control despite being designed for the same phase margin. In linear control, a greater phase margin is required to dampen the overshoot further, whereas here, it has been achieved with the same amount of phase margin and bandwidth. This improvement might be attributed to the presence of a lead element ahead of the nonlinear element (Cai et al., 2020; van den Eijnden et al., 2020).

The subtle differences between HIGS and FO-HIGS may stem from their use of lead elements with varying orders, as exemplified in (Karbasizadeh, 2023, Chapter 9) in the context of reset control systems. Additionally, the inclusion of a parallel linear element in HIGS (Case 1) could contribute to these variations. Future research should delve deeper into this aspect to ascertain the underlying reasons for the observed differences.

In Section 3.2, we have analytically derived that the FO-HIGS element remains within its upper gain-region in the steady-state solution when exposed to a single sinusoidal input with a frequency $\omega \leq \omega_{\mathrm{L}}$. To validate whether this behaviour is still observed in closed-loop, we consider the same closed-loop control systems as considered in the step response example, but now with an input $r(t) = \sin(\omega_{\mathrm{in}}t)$.
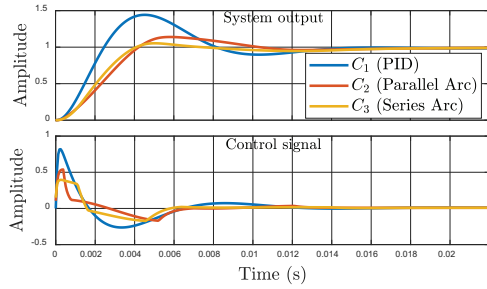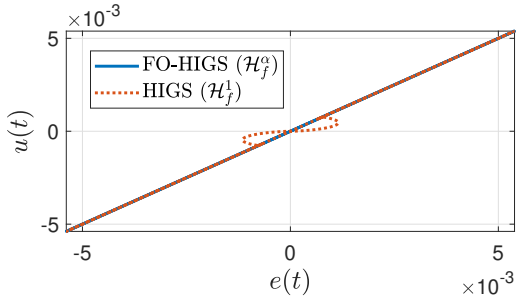
Fig. 6. Step responses of the three control systems.

Fig. 7. Trajectory of the output of FO-HIGS and HIGS in the e-u plane.

In Fig. 7, the e-u plane for HIGS and FO-HIGS are depicted for an input frequency $\omega_{\text{in}} = 2\pi \times 2.5 \,\text{rad/sec}$. Note that this frequency is lower than $\omega_{\text{L}} = 2\pi \times 4.8$ rad/sec, as can be derived from (13) when substituting the parameter values corresponding to controller C_3. From Fig. 7 it is evident that the FO-HIGS element stays in the upper gain-region for all time in one period, whereas the HIGS element operates in both the gain- and integrator-region.

6. CONCLUSION

In this paper we propose a modified FO-HIGS, designed to exhibit absolute gain behavior below a specified frequency ω_L. Through analytical derivation, we establish the HOSIDF of this modified system, demonstrating the absence of higher-order harmonics at frequencies below ω_L. Notably, when $\alpha = 1$, corresponding to the classical HIGS, this desired behavior is absent. However, for values of $\alpha < 1$, the system can exhibit such desired behavior. In addition, this paper involves incorporating the novel FO-HIGS element, along with a lead, to create a CgLp filter with tunable phase. This filter is then tuned for controlling a second-order system, and the results are compared with classical HIGS and PID controllers. As anticipated, the transient response aligns with that of HIGS, showing improvement over PID, while the steady-state (below ω_L) exhibits pure gain behavior, confirming the validity of our theory in the closed-loop system.

Looking ahead, our future work will delve into the frequency-domain stability analysis of closed-loop systems containing an FO-HIGS element. Furthermore, we will focus on developing a frequency-domain tuning method while taking noise and disturbances into account.

REFERENCES

Cai, C., Dastjerdi, A.A., Saikumar, N., and HosseinNia, S.H. (2020). The optimal sequence for reset controllers. In *Proc. Eur. Control Conf. (ECC)*, 1826–1833.

Deenen, D., Heertjes, M., Heemels, W., and Nijmeijer, H. (2017). Hybrid integrator design for enhanced tracking in motion control. In *Proc. Amer. Control Conf. (ACC)*, 2863–2868.

Deenen, D.A., Sharif, B., van den Eijnden, S., Nijmeijer, H., Heemels, M., and Heertjes, M. (2021). Projection-based integrators for improved motion control: Formalization, well-posedness and stability of hybrid integrator-gain systems. *Automatica*, 133, 109830.

Freudenberg, J., Middleton, R., and Stefanpoulou, A. (2000). A survey of inherent design limitations. In *Proc. Amer. Control Conf. (ACC)*, volume 5, 2987–3001.

Hosseini, S.A., Tavazoei, M.S., Van Eijk, L.F., and HosseinNia, S.H. (2022). Generalizing hybrid integrator-gain systems using fractional calculus. In *Proc. IEEE Conf. Control Technol. Appl. (CCTA)*, 1050–1055.

Hunnekens, B., Wouw, N., and Nešić, D. (2016). Overcoming a fundamental time-domain performance limitation by nonlinear control. *Automatica*, 67, 277–281.

Karbasizadeh, N. (2023). *Shaping Nonlinearity in Reset Control Systems to Realize Complex-Order Controllers: Application in Precision Motion Control*. Ph.D. thesis, Delft University of Technology.

Munnig Schmidt, R., Schitter, G., Rankers, A., and van Eijk, J. (2020). *The Design of High Performance Mechatronics: High-Tech Functionality by Multidisciplinary System Integration*. IOS Press.

Nuij, P., Bosgra, O., and Steinbuch, M. (2006). Higher-order sinusoidal input describing functions for the analysis of non-linear systems with harmonic responses. *Mech. Syst. Signal Process.*, 20(8), 1883–1904.

Pavlov, A., Pogromsky, A., van de Wouw, N., and Nijmeijer, H. (2004). Convergent dynamics, a tribute to boris pavlovich demidovich. *Syst. Cont. Lett.*, 52(3), 257–261.

Rijlaarsdam, D., Nuij, P., Schoukens, J., and Steinbuch, M. (2017). A comparative overview of frequency domain methods for nonlinear systems. *Mechatronics*, 42, 11–24.

Saikumar, N., Sinha, R.K., and HosseinNia, S.H. (2019). "constant in gain lead in phase" element– application in precision motion control. *IEEE/ASME Trans. Mechatron.*, 24(3), 1176–1185.

Shchedrin, G., Smith, N.C., Gladkina, A., and Carr, L.D. (2018). Exact results for a fractional derivative of elementary functions. *SciPost Phys.*, 4, 029.

van den Eijnden, S.J.A.M., Heertjes, M.F., Heemels, W.P.M.H., and Nijmeijer, H. (2020). Hybrid integrator-gain systems: A remedy for overshoot limitations in linear control? *IEEE Control Syst. Lett.*, 4(4), 1042–1047.

van Dinther, D., Sharif, B., van den Eijnden, S., Nijmeijer, H., Heertjes, M., and Heemels, W. (2021). Overcoming performance limitations of linear control with hybrid integrator-gain systems. *IFAC-PapersOnLine*, 54(5), 289–294.

van Eijk, L.F., Beer, S., van Es, R.M.J., Kostić, D., and Nijmeijer, H. (2023). Frequency-domain properties of the hybrid integrator-gain system and its application as a nonlinear lag filter. *IEEE Trans. on Control Syst. Technol.*, 31(2), 905–912.

Zhao, G., Nešić, D., Tan, Y., and Hua, C. (2019). Overcoming overshoot performance limitations of linear systems with reset control. *Automatica*, 101, 27–35.